Available online at www.sciencedirect.com
SCIENCE DIRECT
Polymer 46 (2005) 8805–8818
polymer
www.elsevier.com/locate/polymer

Effect of in situ prepared silica nano-particles on non-isothermal crystallization of polypropylene

Sachin Jain[a,c], Han Goossens[a,c,*], Martin van Duin[b,c], Piet Lemstra[a,c]

[a]*Department of Polymer Technology, Faculty of Chemical Engineering and Chemistry, Eindhoven University of Technology, P.O. Box 513, 5600 MB Eindhoven, The Netherlands*
[b]*DSM Research, P.O. Box 18, 6160 MD Geleen, The Netherlands*
[c]*Dutch Polymer Institute, P.O. Box 902, 5600 AX Eindhoven, The Netherlands*

Received 13 October 2004; received in revised form 3 December 2004; accepted 15 December 2004
Available online 12 July 2005

Abstract

The crystallization behavior of PP/silica nanocomposites prepared in-situ via solid-state modification and sol–gel reaction is investigated. The crystallization behavior studied with DSC shows that in situ formed silica nano-particles act as nucleating agents. The non-isothermal crystallization kinetics of PP/silica nanocomposites is studied using a combined Avrami–Ozawa approach and shows a two-stage crystallization process: the primary stage is characterized by nucleation and spherulitic growth and the secondary stage is characteristic of the perfectioning of crystals. Silica speeds up the primary stage, resulting in a more narrow lamellar thickness distribution. The crystallization activation energy decreases with increasing silica content in the PP/silica nanocomposites. The nucleating efficiency of the in-situ prepared silica particles based on the scale as proposed by Lotz and co-workers is found to be 20% in the low concentration range and is higher compared to silica nano-particles as well as other nano-fillers studied. The melting behavior indicates the formation of more perfect crystals with a narrow lamellar thickness distribution and the WAXD patterns show that silica nano-particles induce the formation of crystals with the β-modification in PP at high silica content (ca. 5 wt%). DMTA analysis shows a marginal lowering of the T_g and an increased mobility of the amorphous phase.

Keywords: Non-isothermal crystallization; Polypropylene nucleation; Silica nano-particles

1. Introduction

Inorganic particle-filled nanocomposites of semi-crystalline polymers have been explored extensively in recent years, especially to improve the mechanical properties, notably modulus and tensile strength [1–4]. The preparation of nylon-clay nanocomposites by Toyota researchers [5] sparked an enormous interest amongst researchers to make high-performance nanocomposites with low-cost inorganic fillers.

The intrinsic properties of semi-crystalline polymers strongly depend on their crystalline morphology. The difficulty in understanding the deformation behavior of semi-crystalline polymers arises from their two-phase structure, i.e. crystalline and amorphous phase; the latter can be subdivided into a mobile and a rigid amorphous phase. In this respect, the effect on the yield stress and strain hardening has been a subject of extensive discussion. Strobl et al. [6] and Schrauwen et al. [7] reported that the yield stress is dominated by crystallinity and the lamellar thickness, while the strain hardening modulus depends mainly on the crystallization conditions and the resultant entanglement density of the amorphous phase. The state of the entangled amorphous phase originates from the crystallization process, since it allows the rearrangement of chains during folding and perfection. This 'reeling in' of polymer chains during crystallization leads to disentanglement of the chains in the melt or amorphous phase [8,9]. The effect is more pronounced for lower cooling rates, resulting in a lower entanglement density and, consequently, a lower strain hardening modulus. Schrauwen et al. [7] showed that the yield stress at which slip of the lamellae is reached depends on both the crystallinity and lamellar thickness. The influence of the crystallization kinetics on the tensile

* Corresponding author. Tel.: +31 40 2473899; fax: +31 40 2436999.
E-mail address: j.g.p.goossens@tue.nl (H. Goossens).

0032-3861/$ - see front matter © 2005 Elsevier Ltd. All rights reserved.
doi:10.1016/j.polymer.2004.12.062

modulus and yield stress of PP was also studied by Dasari et al. [10]. However, at higher strains the entangled amorphous phase dominates the deformation process. A higher entanglement density implies that a higher stress is generated when the material is stretched. These findings can even have a more pronounced effect in case of polymers with nucleating additives [11].

In this context, it is important to note that the crystallization kinetics and crystalline morphology of semi-crystalline polymer and their nanocomposites strongly depend on the processing conditions [12–14]. Filler particles can influence the flow and hence the crystallization behavior and final morphology during processing. Industrial polymer processes, such as extrusion, injection molding, and film blowing, are operated under dynamic, non-isothermal conditions. To study effect of the complex thermal conditions during processing, it is important to investigate the behavior of PP-nanocomposites during non-isothermal crystallization [15]. Although numerous investigations were carried out on isothermal crystallization of PP with nucleating agents and of PP-nanocomposites [16–19], very few studies have been published related to non-isothermal crystallization of PP-nanocomposites [20–22].

Isothermal crystallization is an idealized crystallization process for which the Avrami theory has been well established to describe the crystallization kinetics [23,24]. Effects of cooling rate and thermal gradients within the sample are avoided in the isothermal crystallization process, whereas conditions are continuously changing in non-isothermal crystallization. The Avrami equation was thus modified to accommodate the changing temperature (environment) [25,26]. Ozawa [27] extended this modified equation by incorporating the effect of the cooling rate, assuming that the crystallization proceeds at a constant cooling rate. Despite these corrections, these methods can still not fully explain the non-isothermal crystallization kinetics of polymers. Liu et al. [28] developed a new approach by combining the Avrami and Ozawa theories and described successfully the non-isothermal crystallization of poly(ether ether ketone) (PEEK).

Table 1 summarizes the findings of some studies on PP-nanocomposites and PP with nucleating agents. Commercial nucleating agents are mostly used in a concentration range below 1 wt%, above which their efficiency reaches a plateau level. This is one of the reasons for concentrating at low filler levels (only up to 1 wt%) in this study. However, the mechanism of nucleation and the concomitant morphology during crystallization are different.

As mentioned earlier, the amorphous phase of PP in these nanocomposites is also affected during processing [29]. It was observed in PP/talc (micro-fillers) systems that the nucleating effect of the filler lowers the glass transition temperature (T_g) resulting in an amorphous phase with a higher mobility [30]. This stresses the importance to study the effect of filler particles on the entanglement density and mobility of the amorphous phase, since it strongly influences the strain hardening behavior [31,32]. The presence of an interfacial layer between the bulk polymer and the filler surface has been well established by various techniques. Therefore, it can be expected that nano-particles with their surface-to-volume ratio may influence the bulk properties [33].

In this paper, we investigate the effect of in-situ formed silica nano-particles on the non-isothermal crystallization kinetics of PP/silica nanocomposites. We use the combined Avrami–Ozawa approach as developed by Liu et al. [28]. The crystallization activation energy was evaluated using Kissinger's method [34]. The nucleation efficiency based on the efficiency scale as proposed by Lotz and co-workers [35] is also calculated to investigate the effectiveness of the silica nano-particles as nucleating agents. The melting behavior of PP/silica nanocomposites is studied by DSC to probe the recrystallization and phase transformation/modifications in these PP-nanocomposites. X-ray diffraction studies were carried out to examine the presence of various crystal forms to explain the DSC melting curves. Further, the effect of silica nano-particles on the T_g and the amorphous phase is investigated by DMTA.

2. Experimental section

2.1. Materials

Porous isotactic polypropylene (PP) having a porosity of $S_{BET(Kr)} = 0.0678\ m^2/g$ was supplied in powder form by Euro-Sabic, The Netherlands. The weight-average molecular weight of PP was 400 kg/mol. The powder was free of antioxidants and stabilizers and stored at −10 °C in the dark. Tetraethoxy orthosilicate (TEOS) was obtained from Aldrich Chemicals. Ammonium hydroxide (NH_4OH) [28% NH_3 in water] obtained from Aldrich Chemicals was used as catalyst for the sol–gel reactions.

2.2. Synthesis of nanocomposites

PP/silica nanocomposites were prepared by the sol–gel method according to the procedure described in our previous work [36]. TEOS was added to the PP powder in the reactor and stirred for about 30 min at 60 °C. After dispersion of TEOS, a mixture of water and ammonium hydroxide was added slowly at a controlled rate to the reactor with continuous stirring under a nitrogen atmosphere. The molar ratio of TEOS/H_2O was 1:5 and a concentration of NH_4OH was 1 wt% on TEOS. The sol–gel reaction was carried out in the reactor at 60 °C for 3 h with continuous stirring. The thus formed sol in PP is then gelled at 80 °C for 5 h under a nitrogen atmosphere, dried under vacuum at 100 °C for 24 h, and subsequently stored at −4 °C in the dark. The samples were physically mixed with antioxidants (concentration of 0.5 wt%) using a powder blender before any further treatment and dried under

Table 1
Crystallization and nucleation data for PP-fillers and nucleating agents from literature

Researchers	Filler (wt%)	T_c (°C)	NE[a] (%)
Quian et al. 2004 [21] PP/nano SiO_2 (typical size ~16 nm)	0	117	0
	1	117.1	0.5
	3	118.8	8.5
	5	121.2	20
Lin et al. 2004 [22] PP/nano-$CaCO_3$ (typical size ~40–60 nm)	0	117.5	0
	2	116.1	0
	5	116.8	0
	10	120.8	16
Kristiansen et al. 2003 [11] PP/DMDBS [bis(3,4-dimethyl benylidene sorbitol)[b]	0	113	0
	0.2	113.5	2
	0.4	120	28
	0.6	127	56
Gui et al. 2003 [18] PP/NA-40 (12H-dibenzo[d,g][1–3] dioxaphosphocin, 2,4,8,10-tetrakis (1,1-dimethylethyl)-6-hydroxy-6-oxide, sodium salt)[b]	0	117	0
	0.2	127	47
	0.4	128	52
	0.6	128	52
Xu et al. 2002 [20] PP/montmorillonite	0	110	0
	3	115	17.8
Pozsgay et al. 2002 [17] PP/montmorillonite (vol%)	0	112	0
	2	117	19
	5	119	27
	10	121	34.6
Lotz et al. 1994 [32]			
PP		114.2	0
DBS (dibenzylidene sorbitol)[b]	0.4	123.2	41
Talc	1	121.4	32
9-fluorene carboxylic acid[b]	1	119.4	18
2,4 (bis butylamine) 6-hydroxy 1, 3, 5 triazine[b]	1	115.5	5

[a] Calculated based on the scale defined in this study (with lower limit for pure PP and upper limit as 138 °C, approximately observed for different grades of PP).
[b] Commercial nucleating agents.

vacuum at 100 °C before chemical and structural characterization.

2.3. Differential scanning calorimetry (DSC)

The crystallization and melting characteristics and the nucleation efficiency were investigated with a TA Instruments Q1000 differential scanning calorimeter, calibrated with Indium for temperature and heat of fusion. Sample weights between 3 and 4 mg were used in standard aluminum pans. The analysis was conducted under standard heating and cooling rates of 10 °C/min unless otherwise indicated.

The non-isothermal crystallization kinetics of these samples were investigated by conducting cooling scans at rates of 2.5, 5, 10, 15, 20 and 30 °C/min from 225 to 30 °C. Prior to the heating or cooling scan, the samples were held at 225 °C for 5 min under a nitrogen atmosphere to erase the thermal history and prevent self-seeding of PP.

The nucleating efficiency is based on the calorimetric efficiency scale proposed by Lotz and co-workers [35] and is calibrated according to their procedure based on the 'ideally' nucleated polymer attainable via self-nucleation. Two limits need to be defined: the lower limit refers to the virgin (non-nucleated) PP and the upper limit to an optimally self-nucleated PP. The nucleation efficiency is a percentage of the range defined by the two limits and is expressed as:

$$\mathrm{NE} = \frac{T_c - T_{c1}}{T_{c2max} - T_{c1}} \times 100 \quad (1)$$

where T_{c1} and T_{c2max} are the crystallization temperatures of the virgin and best self-nucleated PP, respectively. T_c is the crystallization temperature obtained in the presence of the nucleating agent (in this case silica). NE is thus equal to 0 for a non-nucleating action and 100 for the optimum efficiency.

Self-nucleation is carried out by heating PP to a selected temperature (T_s). When T_s is located in the melting range, the formation of stabilized polymer crystal fragments occur. The self-nucleation procedure as applied in DSC runs is shown in Fig. 1. The heating and cooling rates are 10 °C/min. The procedure essentially involves four steps.

Step A. Complete melting of samples at 225 °C for 10 min to erase the previous thermal history. This step eliminates most of the nuclei.

Step B. Creation of the standard state (T_{c1}) by cooling from (A) at the pre-determined cooling rate of 10 °C/min to some low temperature T_1 (~30 °C). The crystallization takes place at the lower limit of the crystallization range

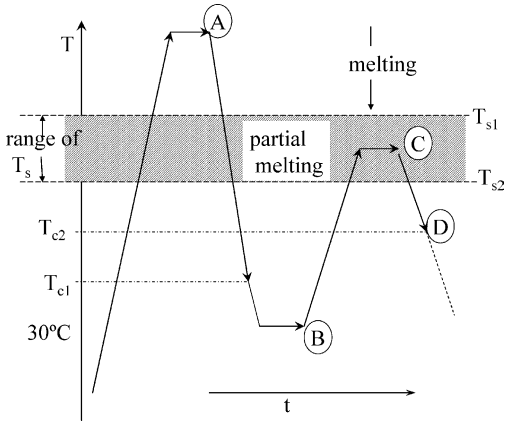

Fig. 1. Self-nucleation procedure as applied in DSC runs (Fillon et al. [35]), (A) complete melting of sample to eliminate most nuclei, (B) creation of standard state, (C) self-nucleation step, and (D) crystallization step.

(T_{c1}). T_{c1} depends on the molecular characteristics of the polymer and decides the lower limit of the nucleation efficiency scale.

Step C. This self-nucleation step is carried out by heating the sample to selected temperatures (T_s). When T_s is located in the partial melting zone (hatched section in Fig. 1), the formation of stabilized crystal fragments occurs. The concentration of these crystal fragments increases with decreasing T_s and reaches saturation at $T_s = T_{s2}$.

Step D. This second crystallization step is achieved by subsequent cooling of the samples which give crystallization peaks at temperature T_{c2} ($T_{c2} \geq T_{c1}$). An increase in T_c indicates an increase in the concentration of nucleation sites induced by the self-nucleation process.

The virgin sample crystallizes at T_{c1}, whereas the best nucleated sample crystallizes at the higher crystallization temperature T_{c2max}. These two extremes decide the limits of the nucleation efficiency scale.

2.4. Dynamic mechanical thermal analysis (DMTA)

Glass transition temperatures and moduli of the samples were measured using a TA Instruments Q800 dynamic mechanical analyzer fitted with a single cantilever geometry. Samples were extruded in a twin-screw mini-extruder with a residence time of 5 min at 190 °C; the rotor speed was set at 50 rpm. The extruded samples were compression into sheets and bars of approx. $20 \times 15 \times 1$ mm^3 size were cut from the sheets. For the measurements, the samples were cooled to −80 °C and held for 5 min and subsequently heated to 100 °C at 2 °C/min. A dynamic force of 0.25 N oscillating at 1 Hz and amplitude of 0.2 μm was used.

Three parameters, i.e. loss tangent (tan δ), the intensity of the transition (S) and full-width at half maximum (FwHM), were used to evaluate the glass transition temperature and the state of the amorphous phase in the samples. The maximum of the transition in the loss tangent (tan δ) curve is taken as the T_g [37]. The intensity of the transition (S) is an important parameter reflecting the mobility and content of the amorphous phase [30]. It is defined as:

$$S = \frac{E'_a - E'_d}{E'_d} \quad (2)$$

where E'_a and E'_d denotes the storage modulus before and after the transition, respectively. A higher S means a higher mobility (less entanglement) or a higher content of amorphous phase. The full-width at half maximum (FwHM) refers to the homogeneity of the amorphous phase. A higher value of FwHM compared to base materials implies a higher inhomogeneity.

2.5. X-ray diffraction

Wide-angle X-ray diffraction (WAXD) experiments were performed at the DUBBLE (Dutch–Belgium) beamline at the European Synchrotron Research Facility (ESRF), Grenoble, France. An X-ray wavelength of 1.218 Å was used. The WAXD patterns were detected by a curved linear microstrip-gas chamber detector. The diffraction angles at the WAXD detector were calibrated with Si powder. The nanocomposites films/powder were put in aluminum pans, and placed in a THMS600 hot stage (Linkam Scientific Ltd) for X-ray diffraction. Data were recorded while the sample was heated and cooled at 10 °C/min. Diffraction patterns were taken at every 6 s, which corresponds to one diffraction pattern for each degree Celsius in the temperature ramp.

2.6. Mechanical properties

Mechanical properties were measured on a Zwick Z010 series universal testing machine in tensile mode. The samples were extruded and injection molded in dog-bone shaped bars of $1.5 \times 5 \times 55$ mm^3. The measurements were done at a cross-head speed of 10 mm/min at room temperature.

3. Results and discussion

The silica nano-particles used in this study are in-situ formed silica particles of 30–80 nm as observed by transmission electron microscopy. The silica particles have hydroxy-groups on its surface as found from MAS ^{29}Si NMR [36]. PP/silica nanocomposites with silica contents up to 5 wt% were used in this study, but we concentrate on the concentration range up to 1 wt%.

3.1. Crystallization behavior

As an example, the crystallization curves of PP and PP/silica nanocomposites at a cooling rate of 10 °C/min are

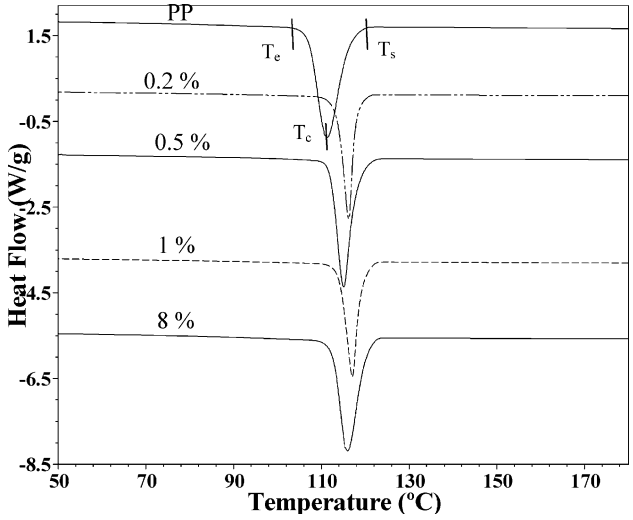

Fig. 2. DSC cooling scans of PP/silica nanocomposites from melt at 10 °C/min as a function of silica content.

shown in Fig. 2. The increase of the crystallization peak temperature (T_c) upon increasing silica content shows the nucleating effect of silica on PP crystallization up to 1 wt% silica, at higher concentration it decreases slightly and remained constant. Table 2 shows the crystallization data at various cooling rates. As the cooling rate is increased, T_c is shifted to lower temperatures for both PP and PP/silica nanocomposites, which may be due to a larger supercooling at higher cooling rates. However, these measurements were performed on pressed films of 3–4 mg. Temperature gradient in the samples are, therefore, not expected. At a given cooling rate, T_c of silica-filled PP is higher than that of pure PP. The overall crystallization time (t_c) was calculated using the following equation:

$$t_c = \frac{(T_s - T_e)}{\beta_0} \tag{3}$$

where β_0 is the rate of cooling, T_s is the initial crystallization temperature and T_e is the final crystallization temperature.

Fig. 3 shows that t_c is reduced upon increasing the silica content at different cooling rates. The increase in T_c and the decrease in t_c are typical characteristics of nucleation-controlled polymer crystallization [38]. Usually, homogeneous nucleation starts spontaneously below the melting temperature [35] and proceeds rather slowly, whereas the heterogeneous crystallization starts as soon as the crystallization temperature is reached. The crystallization of silica nano-particles filled PP proceeds mainly via heterogeneous nucleation by the silica nano-particles. However, two regions, i.e. below and above approximately 1 wt% of silica, can be distinguished showing a different nucleating effect. The DSC-experiments at different cooling rates apparently show the same trend, except at the highest cooling rate, i.e. 50 °C/min. Since, for each cooling rate a different sample was used, the repeatability seems sufficient to draw conclusions. The apparent decrease in nucleation

Table 2
Non-isothermal crystallization behavior of PP/silica nanocomposites at different cooling rate

Silica content	0%			0.20%			0.50%			1.00%			1.50%			2.00%		
cooling rate (°C/min)	T_s (°C)	T_c (°C)	T_e (°C)	T_s (°C)	T_c (°C)	T_e (°C)	T_s (°C)	T_c (°C)	T_e (°C)	T_s (°C)	T_c (°C)	T_e (°C)	T_s (°C)	T_c (°C)	T_e (°C)	T_s (°C)	T_c (°C)	T_e (°C)
2.5	126	118	107	129	118	110	125	121	118	130	122	117	122	118	116	127	123	120
5	123	115	108	125	116	113	122	118	116	125	119	114	118	117	114	124	120	117
10	120	111	102	124	114	106	116	115	107	126	118	107	117	115	111	121	116	112
15	119	113	90	123	113	96	117	115	109	127	116	100	115	112	106	119	114	110
20	118	112	85	124	112	92	116	114	106	124	115	92	114	111	103	117	113	107
25	118	111	85	121	111	89	115	114	108	122	115	87	113	110	102	116	112	107
30	119	106	82	119	110	89	115	112	105	121	114	91	113	110	102	114	110	103
50	116	105	76	115	108	83	112	110	102	116	112	85	111	107	100	111	107	100

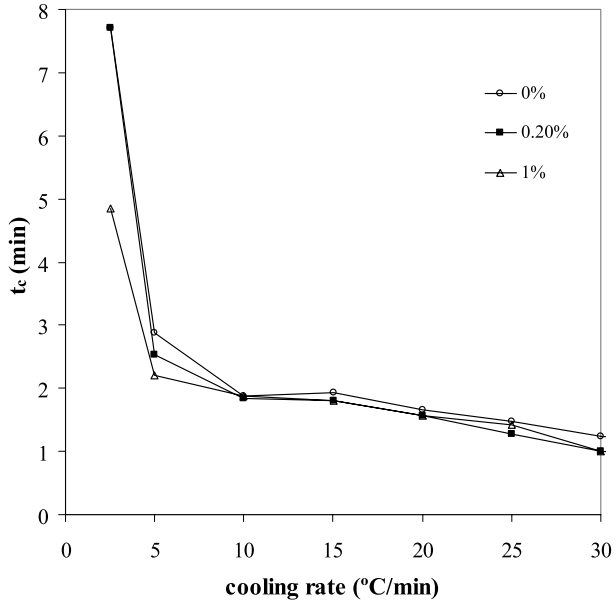

Fig. 3. Overall crystallization time versus cooling rate of PP/silica nanocomposites as a function of silica content.

may be related to a different nucleation mechanism and to the volume fraction of silica particles. We have no conclusive explanation for these observations and more experiments with different characterization techniques are needed to elucidate the behavior.

The degree of crystallinity at the peak melting temperature is calculated from the melting heat [ΔQ_m (J/g)] obtained from the DSC measurements according to the following equation (after normalization for the PP concentration):

$$X_c = \frac{\Delta Q_m}{\Delta H_0} \tag{4}$$

where $\Delta H_0 \approx 207.1$ J/g is the melting enthalpy of 100% crystalline PP [31].

The degree of supercooling and the degree of crystallinity of PP/nanocomposites with varying silica levels at a cooling rate of 10 °C/min are listed in Table 3. The degree of supercooling is defined as the difference in the melting peak temperature (T_m) and crystallization peak temperature (T_c) at a given cooling rate. The nucleating effect of silica results in a shifting of T_c to higher temperatures, whereas T_m is hardly affected indicating that the supercooling (ΔT) is reduced with increasing silica content followed by a slight increase at higher concentration. When a polymer crystallizes with less supercooling, it crystallizes more perfectly.

From the DSC curves, the values of the relative crystallinity at various cooling rates can be calculated. The relative crystallinity as a function of time can be defined as:

$$X_t = \frac{X_t}{X_\infty} = \frac{\int_{t_0}^{t} \left(\frac{dQ}{dt}\right) dt}{\int_{t_0}^{t_e} \left(\frac{dQ}{dt}\right) dt} \tag{5}$$

where (dQ/dt) represents the rate of heat flow, X_t and X_∞ represent the crystallinity at time t and at the end of crystallization process (t_e), respectively.

For the non-isothermal crystallization process, the crystallization time t and temperature T are related as:

$$t = \frac{|T_0 - T|}{\beta_0} \tag{6}$$

where T is the temperature at time t and T_0 is the initial temperature when crystallization starts. Thus, the relative crystallinity as a function of temperature (T), $X_c(T)$, is defined as:

$$X_c(T) = \frac{\int_{T_s}^{T} \left(\frac{dQ(T)}{dT}\right) dT}{\int_{T_s}^{T_e} \left(\frac{dQ(T)}{dT}\right) dT} \tag{7}$$

The relative crystallinity as a function of time and temperature for PP and PP/silica nanocomposites is shown in Fig. 4. All curves have similar sigmoidal shapes. The curvature of the upper parts (near complete crystallization) in the plots is due to the spherulitic impingement in the later (growth) stages of crystallization. From the curves in Fig. 4, the half-life times to reach 50% crystallinity ($t_{1/2}$) of non-isothermal crystallization are calculated and listed in Table 3 for a cooling rate of 10 °C/min. It can be observed that PP in the presence of silica is nucleated at higher temperatures and crystallizes faster. The faster increase of the initial stages of crystallization also signifies the nucleating effect of silica nano-particles.

3.2. Non-isothermal crystallization kinetics

The Avrami equation [23,24] was developed for isothermal crystallization, although it has also been used to study non-isothermal processes [39], and reads as:

Table 3
Crystallization and melting data for PP/silica nanocomposites at a scanning rate of 10 °C/min

Sample		T_c		T_m peak (°C)	ΔT (°C)	$t_{1/2}$ (s)	X_c (%)	Φ
		Peak (°C)	ΔH_c (J/g)					
PP		111.4	99.7	158.7	47.4	64.5	48.1	1.00
PP/silica	0.2%	114.2	102.3	159.8	45.5	55	49.4	0.89
PP/silica	0.5%	117.6	106.5	160.3	42.7	51	51.5	0.78
PP/silica	1.0%	116.2	110.2	160.2	44.0	46	53.7	0.74
PP/silica	1.5%	114.6	100.7	160.0	45.4	32	49.4	0.71

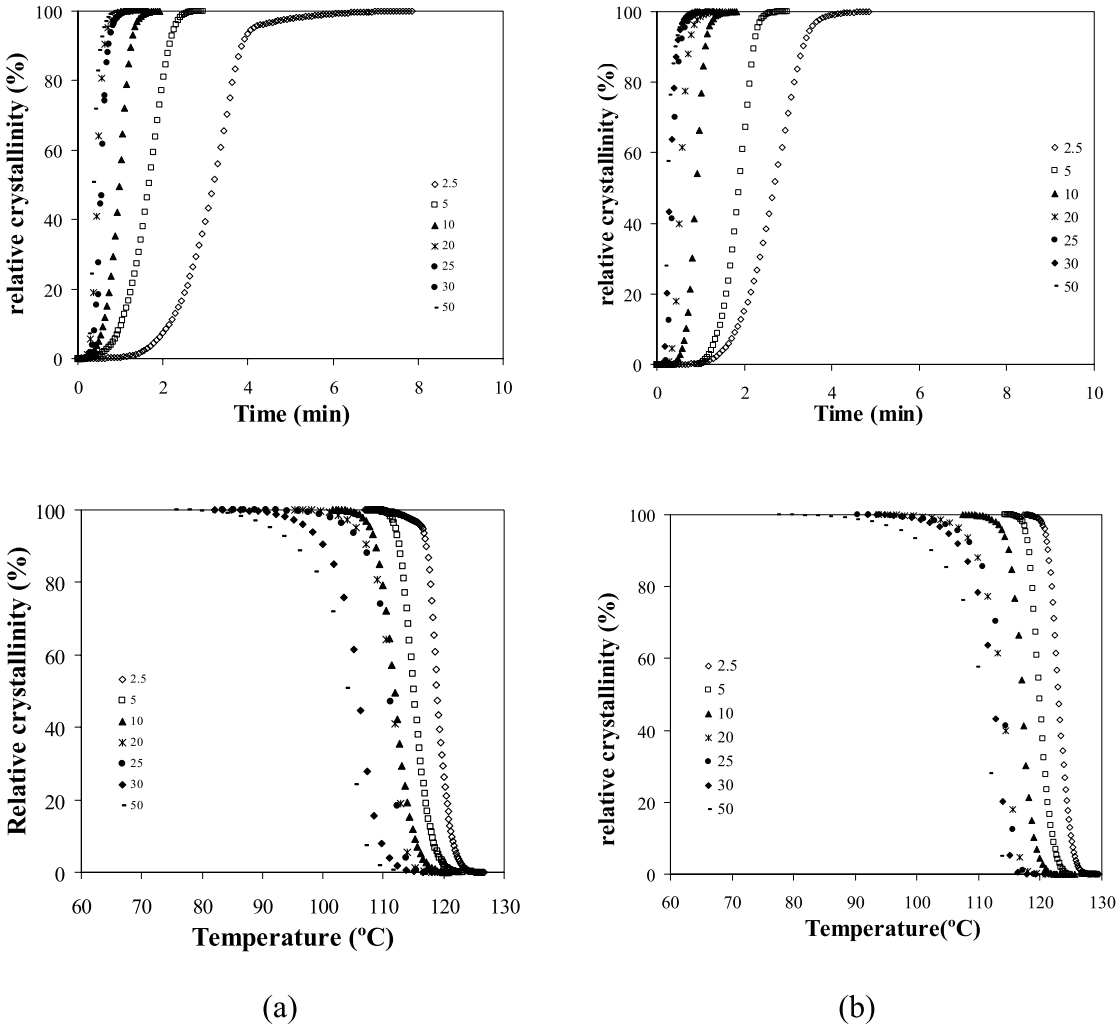

Fig. 4. Relative crystallinity versus time and temperature for non-isothermal crystallization (a) PP and (b) PP/silica (1 wt%) at different cooling rates indicated by the legends.

$$X_t = 1 - \exp(-Z_t(T)t^n) \tag{8}$$

where n is the Avrami exponent, $Z_t(T)$ the Avrami rate constant and X_t the relative crystallinity at time t.

Although the physical meaning of Z_t and n cannot be related to the non-isothermal case in a simple way, their use provides further insight into the kinetics of non-isothermal crystallization. For non-isothermal processes, the Avrami crystallization rate $Z_t(T)$ has been corrected [25,40], since the temperature is constantly changing during the measurements. Thus, the parameter characterizing the non-isothermal crystallization kinetics has been defined as:

$$\log Z_c = \frac{\log Z_t}{\beta_0} \tag{9}$$

where β_0 is the cooling rate.

According to Eq. (8), $\log[-\ln(1-X_t(t))]$ is plotted against $\log t$ in Fig. 5. The values of the Avrami exponent n and the rate parameter Z_c (i.e. corrected Z_t) can be determined from the slope and intercept of the curves, respectively. It is interesting to note that the curves for PP show only one region (secondary crystallization is less significant) as also observed by He et al. [41] and Xu et al. [20]. At high cooling rates, a prominent saturation at higher relative crystallinity is observed. However, for the silica nano-particle filled PP, each curve shows two regions: the so-called primary stage followed by the secondary stage (plateau region). This has not been reported in earlier studies on PP-nanocomposites [20]. Such a behavior has been reported for PEEK by Liu et al. [28] (non-isothermal crystallization), Cebe et al. [39] and Lee et al. [42] (isothermal crystallization). The change from primary to secondary stage occurs near approximately 70% relative crystallinity. Each regime gives different values for n (n_1 and n_2) and Z_c (Z_{c1} and Z_{c2}) as listed in Table 4. For PP, the two stages are not distinct; however, for comparison with the nanocomposites, the curves are split into two stages: below and above 70% crystallinity. The average values of the Avrami exponent for PP are $n_1 = 4.4$ and $n_2 = 2.1$, although the value of exponent n is more scattered than for

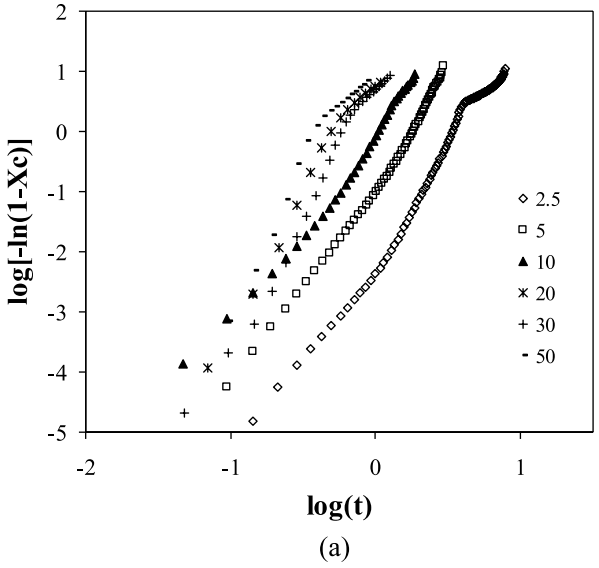

(a)

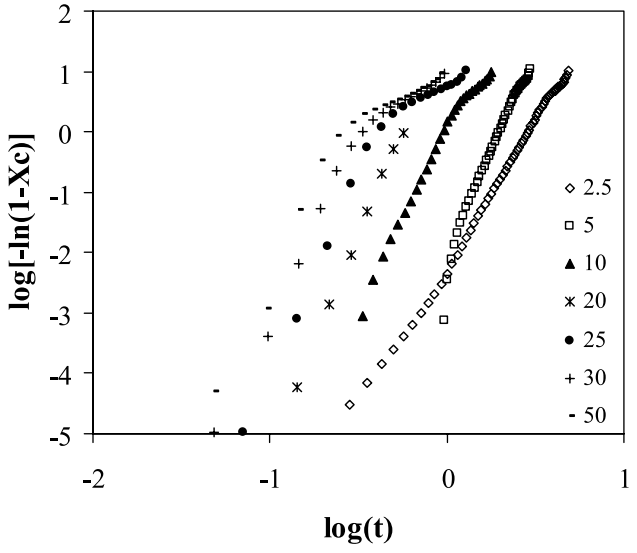

(b)

Fig. 5. Avrami plots of $\log[-\ln(1-X_t(t))]$ versus $\log t$ for non-isothermal crystallization of (a) PP and (b) PP/silica (1 wt%).

isothermal crystallization. Here, $n_1 \approx 4$ correspond to three-dimensional spherical growth and homogeneous nucleation in the primary crystallization stage as normally observed in the case of an isothermal crystallization process; $n_2 \approx 2$ can be assigned to one-dimensional linear growth and a thermal nucleation. For PP/silica nanocomposites, $n_1 \approx 7$ corresponds to solid-sheaf growth from the silica nano-particles (as usually observed in cold-crystallization of polymers [28]) and thermal nucleation during the primary stage. The initial increase and then decrease of the Avrami exponent n with the increasing cooling rate stresses the importance of thermal nucleation in the non-isothermal crystallization process, whereas $n_2 \approx 2$ implies that during the secondary stage, the crystallization proceeds similar to PP with one-dimensional growth and a thermal nucleation.

Generally, the secondary stage is related to crystal perfecting, which is triggered by the initially poorly crystallized molecules or small, imperfect and metastable crystals. However, selective adsorption of PP-chains at the silica particle surface may also play a role. The decrease in n_2 with increasing cooling rate corresponds to a faster or more effective secondary stage, which is mainly caused by the slower primary stage and more imperfect crystals. PP/silica nanocomposites have lower n_2 values than PP at a given cooling rate suggesting a faster secondary crystallization for PP/silica nanocomposites. The primary stage in PP/silica nanocomposites has already proceeded towards higher crystallinity and more perfect crystals than in PP due to the nucleating effect of silica nano-particles. This perfectioning step results in lamellar thickening [7]. The 'reeling in' of polymer chains also occurs during the secondary stage. Schrauwen et al. [7] reported that this results in a more disentangled amorphous phase which eventually affects the mechanical properties. The faster cooling rates are especially important as they closely mimic the most industrial molding processes. If the secondary crystallization is not complete, the product will continuously crystallize over time in turn changing the properties of the product.

The Avrami equation for the non-isothermal crystallization is valid for the early stages of the crystallization only and does not account for the secondary crystallization of the polymers [28,38]. The observations from these Avrami plots are indicative, but not conclusive. The Avrami equation was extended by Ozawa [27] to develop a simple method to study the non-isothermal crystallization kinetics, assuming that the crystallization occurs at a constant rate. According to Ozawa, the relative crystallinity at temperature T, X_T, can be calculated using following equation:

$$1 - X_T = \exp\left[-\frac{K(T)}{|\beta_0|^m}\right] \tag{10}$$

where $K(T)$ is a function related to overall crystallization rate and m is the Ozawa exponent that depends on the dimensions of crystal growth. However, Ozawa's theory neglects the slow secondary crystallization and the dependence of folded chain length (lamellar thickness) on the temperature [43]. Cakmak and Lee [44] and Kim et al. [15] showed that the Ozawa analysis cannot describe the non-isothermal crystallization of polymers in general.

As the degree of crystallinity is related to the cooling rate β_0 and the crystallization time t (or temperature T), the relation between β_0 and t needs to be defined for a given degree of crystallinity. Consequently, Liu et al. [28] derived a new kinetic equation for non-isothermal crystallization by combining Eqs. (8) and (10) yielding:

$$\log Z_t + n \log t = \log K(T) - m \log \beta_0 \tag{11a}$$

Table 4
Values of n and Z_c and $t_{1/2}$ for PP and PP/silica nanocomposites obtained from Avrami analysis for non-isothermal crystallization process

Sample cooling rate (°C/min)	0%				0.20%				1%			
	Primary stage		Secondary stage		Primary stage		Secondary stage		Primary stage		Secondary stage	
	n_1	Z_{c1}	n_2	Z_{c2}	n_1	Z_{c1}	n_2	Z_{c2}	n_1	Z_{c1}	n_2	Z_{c2}
2.5	3.7	0.13	1.8	0.52	4.7	0.08	2.1	0.41	4.6	0.13	4.0	0.41
5	3.4	0.64	4.9	0.55	5.2	0.64	4.2	1.37	7.3	0.37	5.4	0.62
10	2.9	0.95	3.5	1.00	7.8	1.05	2.8	1.05	6.3	1.03	3.2	1.07
15	7.0	1.17	2.6	1.08	8.4	1.18	2.3	1.06	11.3	1.13	2.9	1.06
20	4.7	1.17	2.2	1.09	10.7	1.14	2.6	1.05	6.4	1.02	2.0	1.25
30	4.6	1.07	2.4	1.06	6.0	1.21	1.8	1.07	6.2	1.26	1.8	1.42
50	4.7	1.12	2.0	1.05	5.7	1.17	1.7	1.05	6.3	1.20	1.5	1.42

$$\log a = \log F(T) - b \log t \tag{11b}$$

where $F(T) = [K(T)/Z_t]^{1/m}$ and b is the ratio of the Avrami to Ozawa's exponent, i.e. $b = n/m$. $F(T)$ refers to the cooling rate at unit crystallization time when the system has a definite degree of crystallinity. This designates that $F(T)$ has a physical and practical meaning for non-isothermal crystallization processes, as Z_t has in the isothermal case.

Therefore, the Avrami-equation and Ozawa-equation are combined as suggested by Liu et al. [28]. According to Eq. (11a) and (11b), a plot of $\log \beta_0$ against $\log t$ at particular degree of crystallinity gives a straight line with slope $-b$ and intercept $F(T)$. Fig. 6 shows the plots of $\log \beta_0$ versus $\log t$ at various degrees of crystallinity and values of b and $F(T)$ are calculated for each particular crystallinity and listed in Table 5. At a certain degree of crystallinity, a high value of $F(T)$ indicates that a high cooling rate is needed to reach this degree of crystallinity in a unit time, which is related to the difficulty of the crystallization process for that particular material. Table 5 shows that the value of $F(T)$ increases with increasing crystallinity. However, the $F(T)$ values of PP/silica nanocomposites at a particular degree of crystallinity are lower and the increase in $F(T)$ with the degree of crystallinity is slower than for PP. This demonstrates that the silica nano-particles facilitate the crystallization process. The combined Avrami/Ozawa equations are able to describe the non-isothermal crystallization process for PP and PP/silica nanocomposites.

The cooling rate greatly influences the non-isothermal crystallization process. Considering this, Kissinger [34] proposed a method to determine the activation energy of crystallization by calculating the variation of crystallization temperature as a function of the cooling rate:

$$\frac{\left[\ln\left(\frac{\beta_0}{T_c^2}\right)\right]}{\left(\frac{1}{T_c}\right)} = \frac{-\Delta E}{R} \tag{13}$$

where β_0 is the cooling rate, R is the gas constant and T_c is the peak crystallization temperature. The crystallization activation energies (ΔE) calculated from the slopes of $\ln[\beta_0/T_c^2]$ versus $1/T_c$ (Fig. 7) are: 435, 322, 324, 311 and 358 kJ/mol for 0, 0.2, 0.5, 1 and 1.5 wt% silica, respectively, in PP nanocomposites. The ΔE of the nanocomposites reduced as the silica concentration is increased up to 1 wt%, after which it displays a marginal increase, which implies that the silica nano-particles influence the PP chains to

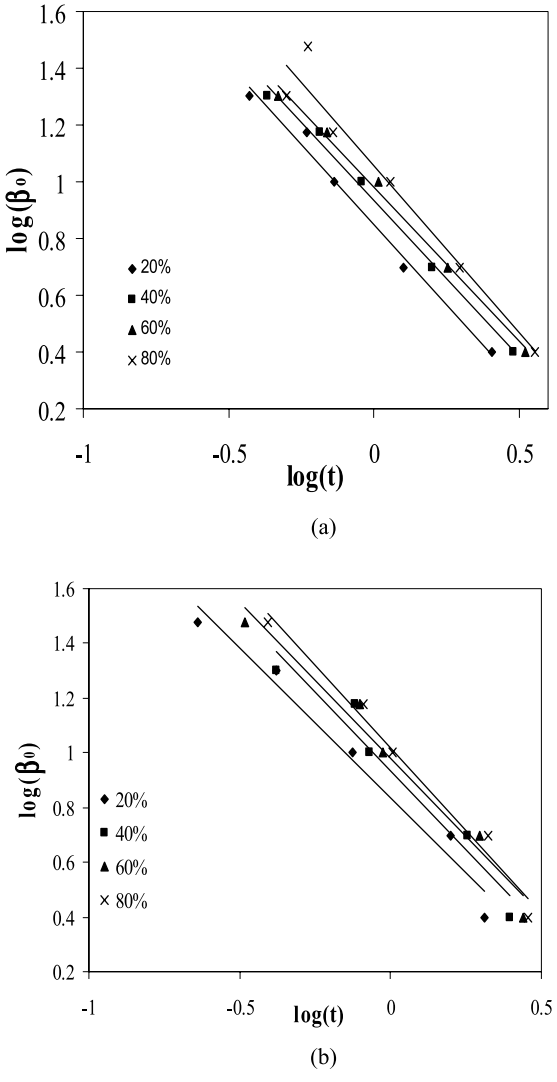

Fig. 6. Log β_0 versus log t from the combined Avrami–Ozawa equation as proposed by Liu et al. for (a) PP and (b) PP/silica (1 wt%).

Table 5
The values of b and $F(T)$ at different degrees of crystallinity calculated from Fig. 7 for PP and PP/silica nanocomposites

$X_c(t)$ (%)		20	40	60	80
Pure PP	b	1.24	1.22	1.19	1.18
	$F(T)$	7.56	9.31	10.46	11.35
PP/silica 0.2%	b	1.2	1.26	1.3	1.13
	$F(T)$	7.41	8.96	9.66	11.3
PP/silica 1%	b	1.09	1.16	1.14	1.21
	$F(T)$	6.58	8.6	9.51	10.45

crystallize easier and accelerate the crystallization rates during the non-isothermal crystallization process.

3.3. Nucleation efficiency

Fig. 8(a) shows the evolution of the crystallization temperature for PP after self-nucleation carried out at different temperatures and fixed cooling rate (10 °C/min). From these curves, T_{c2max} for the best self-nucleated PP is chosen as the upper limit and T_{c1} of the virgin PP is taken as the lower limit. The higher temperature T_{c2max} is 138.6 °C, whereas the lower temperature T_{c1} is 110.6 °C, i.e. a difference of 26.9 °C defines the efficiency scale.

The nucleating efficiency of silica nano-particles is plotted in Fig. 8(b) as a function of silica concentration. It shows a nucleating efficiency close to 20%, which is comparable to most commercially available nucleating agents, independent of the underlying mechanism of nucleation. The in-situ prepared silica nano-particles, as used in this paper, show a higher nucleation efficiency compared to other PP-nanocomposites, including silica (Table 1). The nucleating efficiency, however, saturates above 0.5 up to 1 wt% followed by a slight decrease at higher concentrations. As explained earlier, the reason for the apparent decrease in nucleation efficiency is not clear at this moment and needs to be resolved using different experimental techniques. The saturation at 0.5 wt% is remarkably similar to the concentration threshold for DMDBS as observed by Kristiansen et al. [11].

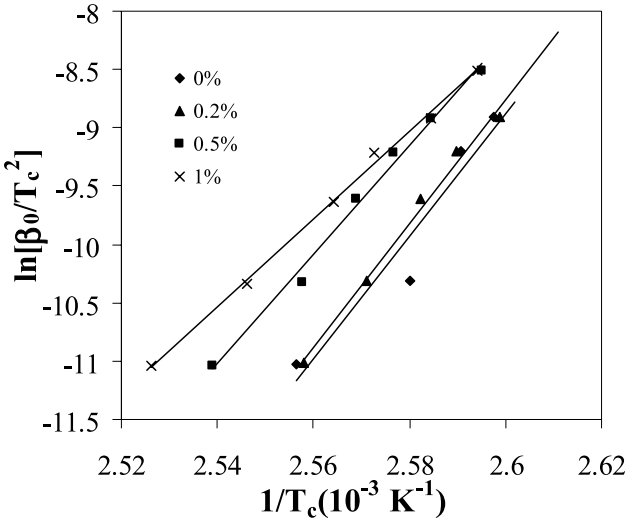

Fig. 7. Kissinger plot for calculating the non-isothermal crystallization activation energies for PP and PP/silica nanocomposites.

3.4. Melting behavior of PP/silica nanocomposites

The melting behavior of the PP/silica nanocomposites reflects the nucleating effect of silica. The narrow melting peaks exhibited by the PP/silica nanocomposites during heating (Fig. 9(a)) suggest that more perfect lamellae are formed with a narrow size distribution. The melting temperature (T_m) is constant but the width of melting peaks, which reflects the lamellar thickness distribution, reduces considerably compared to pure PP. The values of T_m, onset of T_m and start (T_{sm}) and end (T_{em}) of the melting endotherms are listed in Table 6. All samples show a melting temperature of 160 °C, which is the characteristic melting point of the α-phase of PP [26]. A small melting peak at approximately 145 °C is observed, although not clear in Fig. 9(a) for low silica concentrations, but for nanocomposites with high silica loadings it is more prominent. This can be assigned to PP-crystals with the β-modification, which is known to have a melting temperature near 145 °C [45]. This is also confirmed by the X-ray diffraction studies. The melting enthalpy is almost constant for all the samples, which implies that the crystallinity remains constant. However, from the crystallization enthalpy, the PP/silica nanocomposites show a slightly higher crystallinity than PP. The recrystallization process may explain this discrepancy. The completion of melting of the β-modification and the start of the recrystallization in the α-modification (α') occurs simultaneously; the peak due to recrystallization reaches a maximum at 150 °C during the melting process. The area of the peak from the β-modification in the silica-nucleated PP is too small to deconvolute from the peak area due to the recrystallization-melting process of α-form during heating with a standard heating rate.

In case of PP/silica nanocomposites with higher silica loadings in the range of 2–5 wt%, the amount of crystals with the β-modification induced by the silica nano-particles is higher (Fig. 9(b)). The peak at 145 °C corresponding to the β-modification is persistent even after repeated melting and crystallization. This signifies that it is not the effect of thermal treatment or melt memory but a true effect of the silica nano-particles on the PP crystal modification.

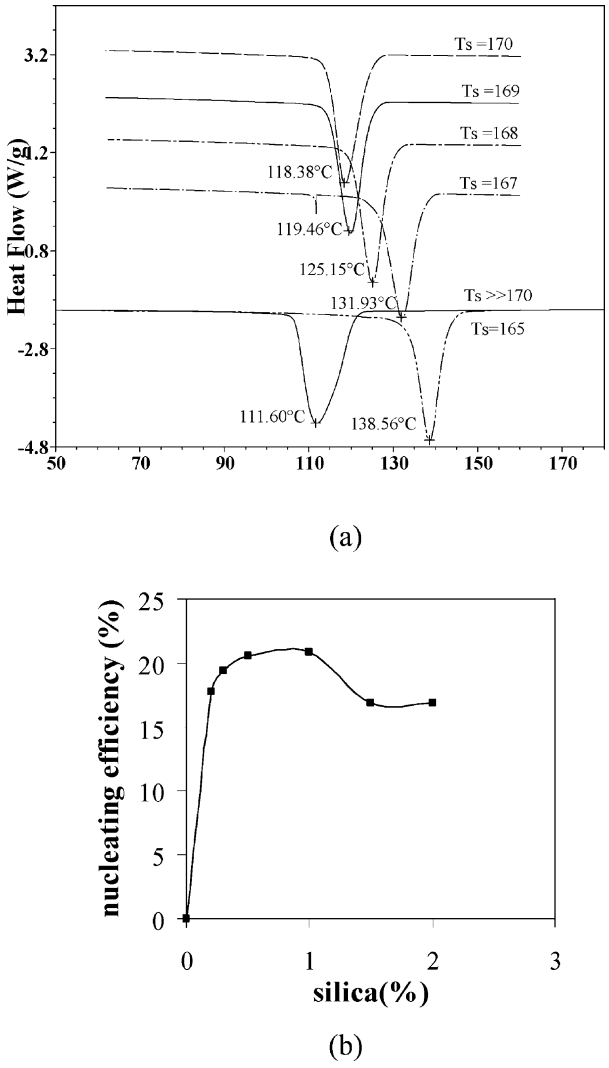

Fig. 8. (a) Cooling curves of PP after melting and annealing for 5 min at various T_s to determine the nucleation efficiency scale, (b) nucleating efficiency as a function of silica content in PP/silica nanocomposites.

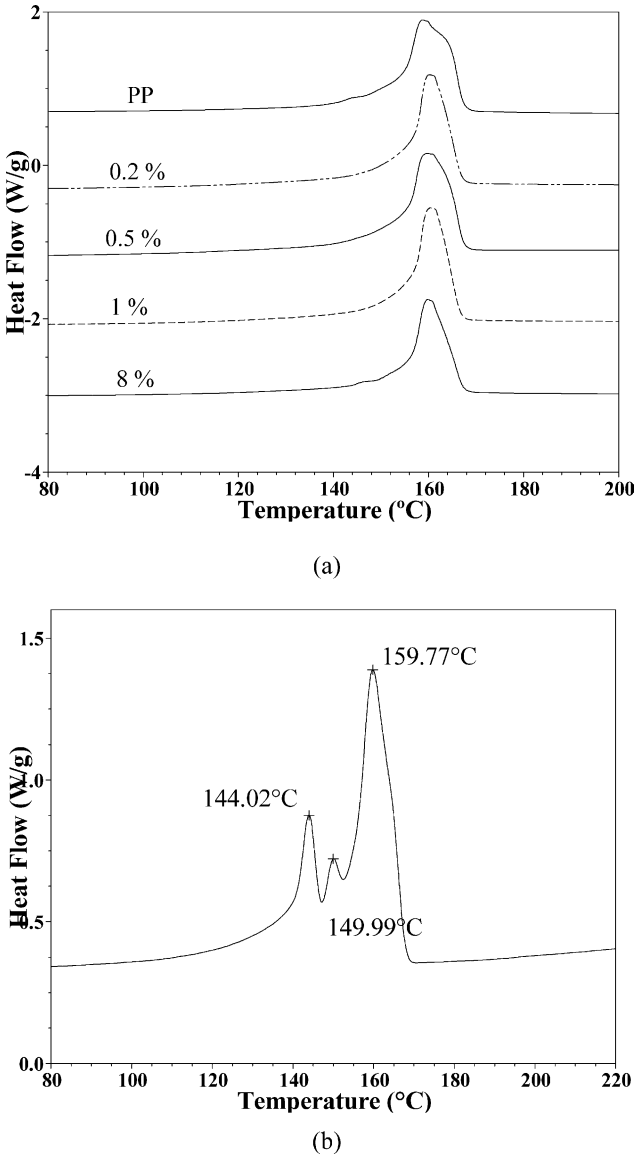

Fig. 9. (a) Melting curves: PP/silica nanocomposites with 10 °C/min, (b) melting curve of PP-nanocomposite with 5 wt% silica to demonstrate the formation of the β-modification.

In situ X-ray diffraction confirms the presence of small β-crystallites in the PP/silica nanocomposites. The WAXD patterns recorded during cooling from the melt (225 °C) to 70 °C at 10 °C/min are shown in Fig. 10. The peak near $2\theta = 16°$ is the characteristic peak of the 300 plane of the β-unit cell [46]. This peak is extremely small in the case of PP, but significantly more intense for silica-nucleated PP. The peaks in the WAXD pattern appear as soon as the material attains an appreciable degree of crystallinity. The appearance of these peaks relates well to the crystallization temperature calculated from DSC cooling curves. The crystallization temperature for PP/silica (1 wt%) nanocomposites is 120 °C, whereas for PP it is 110 °C.

Table 6
Melting data for PP/silica nanocomposites at a heating rate of 10 °C/min

Silica (wt%)	T_m (°C)	$T_{m\ onset}$ (°C)	ΔH_m (J/g)	T_{sm}	T_{em}	ΔT	X_{cm}
0.0	158.7	153.7	91.1	171.0	99.9	71.1	44.0
0.2	159.8	154.7	92.4	169.4	114.5	54.9	44.8
0.5	160.3	156.1	91.8	169.9	127.8	42.1	44.6
1.0	160.2	156.2	93.0	168.7	125.7	43.0	43.4
8.0	159.8	155.6	75.1	170.7	121.8	48.9	39.4

3.5. Effect of silica on the glass transition temperature

As explained earlier, the peak in the tan δ curve is used to determine the glass transition temperature and the intensity of transition calculated from the change in the storage modulus before and after glass transition is used to determine the mobility of the amorphous phase. Fig. 11(a) shows the evolution of the loss tangent (tan δ), which is always higher for the PP/silica nanocomposites than for PP and Fig. 11(b) shows the storage modulus curves. The storage modulus shows a sharp decrease for the PP/silica nanocomposites at the glass transition temperature, but it is still higher than for pure PP.

The T_g for PP/silica nanocomposites is observed at temperatures below that of PP (Table 7). This can be explained with the help of the DSC results: The silica acts as a nucleating agent leading to the formation of more perfect crystals along with a faster crystallization of PP (Table 3). Perfecting of crystals results in a more disentangled amorphous phase which has a higher mobility in the PP/silica nanocomposites, resulting in a slightly lower T_g value. The effect is more evident from the drop in elastic modulus and is further explained by using the intensity of the transition.

The intensity of the transition (S) is higher for the PP/silica nanocomposites than for PP (Table 7). This indicates that the nanocomposites have a less entangled (more mobile) amorphous phase; however, DSC data shows that the nanocomposites have a higher crystallinity than PP. The higher intensity of the transition suggests that the drop in elastic modulus above the glass transition is higher which in turn indicates a more disentangled amorphous phase. Díez-Gutiérrez et al. [30] observed that the T_g as well as the intensity of the transition decreased for PP/talc composites. According to them, the addition of a rigid phase reduces the mobility of polymer chains, which results in lower values of the transition. The concentration of talc used in their work was 40 wt%, whereas in the present work the silica concentration is less than 1 wt% implying that the concentration of the rigid amorphous phase is not high enough to affect the mobility of the polymer chains. However, the kinetics of crystallization in the presence of fillers does affect the amorphous phase.

The inhomogeneity of the amorphous phase and a high mobility imparts the flexibility to the matrix, which results in a decrease of storage modulus at higher temperatures even with a higher crystallinity. An increase of the FwHM values of T_g was observed for PP/silica nanocomposites. This was expected considering the nucleating effect of silica, which results in faster crystallization and more perfect crystals but in a more inhomogeneous amorphous phase than for PP.

The decrease in the strain hardening modulus observed for PP/silica nanocomposites during stretching at higher strains (Fig. 11(c)) is the result of this less entangled, more mobile amorphous phase. The slope of the curves at higher strains can be considered as a measure for the strain hardening modulus.

4. Conclusions

The crystallization behavior as studied with DSC shows that in situ prepared silica nano-particles via the sol–gel method in PP/silica nanocomposites act as nucleating agents. The nucleating efficiency of the silica particles is 20% in the low concentration range and is comparable to the most commercial nucleating agents, and higher compared to silica nano-fillers as well as other nano-fillers studies by other researchers.

The combined Avrami–Ozawa equation approach provides a convenient tool to study the non-isothermal crystallization process for these systems. The non-isothermal crystallization kinetics proceeds in two stages: the primary stage is characterized by nucleation and spherulitic growth and the secondary stage is characteristic of the perfection of crystals. Silica, being a heterogeneous nucleating agent, accelerates the primary stage, resulting in more perfect crystals. This is also evident from the melting behavior of the PP/silica nanocomposites. The crystallization activation energy decreases with increasing silica content in the PP/silica nanocomposites, accelerating

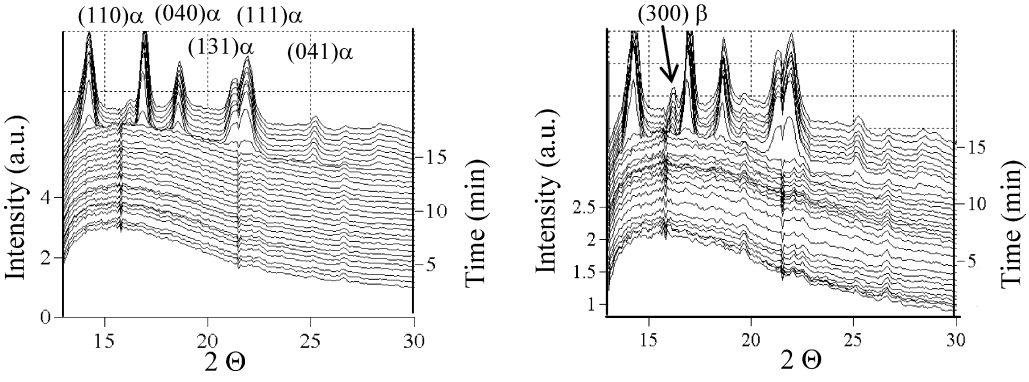

Fig. 10. WAXD patterns of (a) PP and (b) PP/silica (1wt%) obtained during cooling from 225 to 70 °C at 10 °C/min.

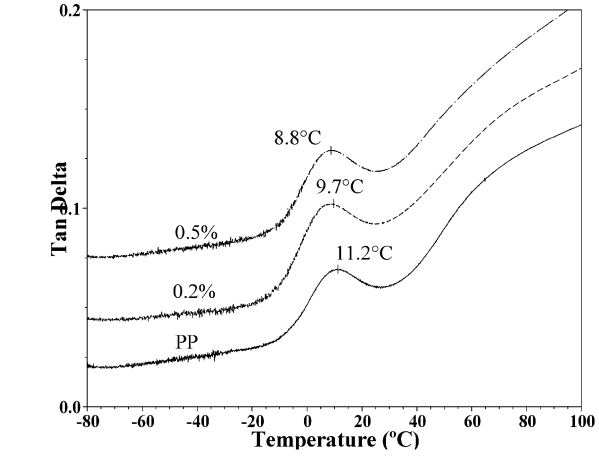

(a)

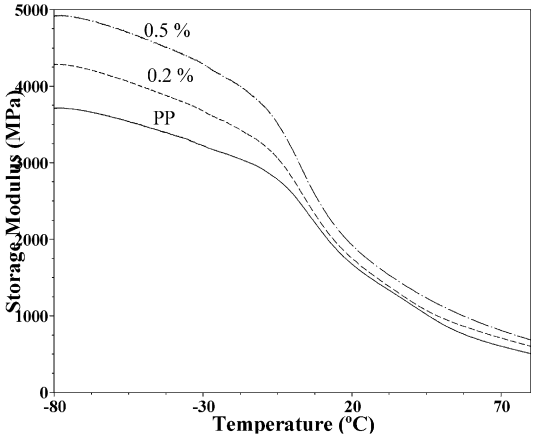

(b)

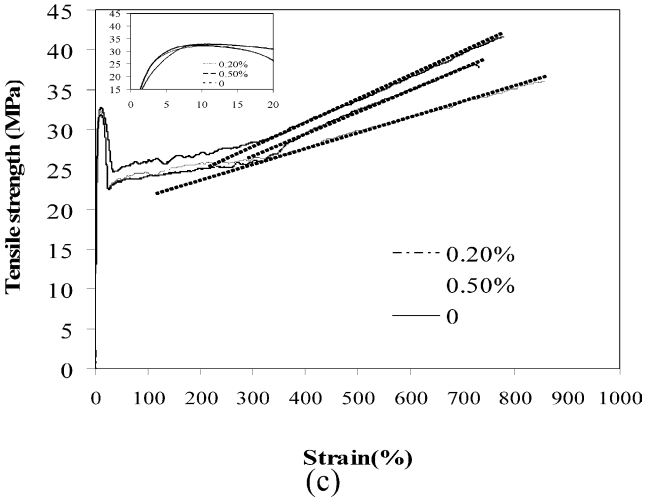

(c)

Fig. 11. The mechanical data for PP/silica nanocomposites as a function of silica content: (a) tan δ as a function of temperature, (b) storage modulus as a function of temperature, (c) stress-strain curves measured at room temperature.

the crystallization. The melting curves indicate the formation of more perfect crystals and a narrow distribution of crystal size and lamellar thickness. The WAXD patterns show that silica nano-particles induce the β-modification in PP. Though at low levels, the presence of some crystals with the β-modification may help in improving the mechanical properties, especially the impact toughness of the PP. DMTA analysis shows a marginal lowering of T_g and an increase in the mobility (less entangled) amorphous phase. The increase in crystallinity results in higher yield stress and the decrease in entanglement eventually results in lower strain modulus. Faster crystallization, higher crystallinity and less entangled amorphous phase as a result of the presence of low concentration of silica nano-particles in PP can form the basis of PP nanocomposites with superior mechanical properties.

Table 7
T_g, intensity of transition and full width at half maximum (FwHM) of PP/silica nanocomposites measured by DMTA

Silica (wt%)	T_g (°C)	S (%)	FwHM (°C)
0	11.2	1.25	38.1
0.2	9.7	1.71	40.7
0.5	8.7	1.82	39.8

Acknowledgements

The authors are grateful to G. W. H. Hőhne for the helpful discussion with interpretation of DSC results and experiments. The authors also thank NWO for research and travel grants for the X-ray synchrotron experiments performed at DUBBLE@ESRF, Grenoble, France. The Dutch Polymer Institute is gratefully acknowledged for sponsoring this investigation under project#133.

References

[1] Bartczak Z, Argon AS, Cohen RE, Weinberg M. Polymer 1999;40:2347.
[2] Giannelis EP, Krishanmoorti RK, Manaias E. Adv Polym Sci 1998;138:107.
[3] Alexandre M, Dubois P. Mater Sci Eng R 2000;28:1.
[4] Argon AS, Bartczak Z, Cohen RE, Muratoglu OK. Toughening of plastics. In: Pearson RA, Sue H-J, Yee AF, editors. ACS symposium series, vol. 759. Washington, DC: American Chemical Society; 2000. p. 98.
[5] Usuli A, Kojima Y, Kawasumi M, Okada A, Fukushima Y, Jurauchi O, et al. J Mater Res 1993;8:1179.
[6] Men Y, Rieger J, Strobl G. Phys Rev Lett 2003;91(9):095502–095511.
[7] Schrauwen BAG, Janssen RPM, Govaert LE, Meijer HEH. Macromolecules 2004;37:6069.
[8] DiMarzio EA, Guttman CM, Hoffman JD. Faraday Discuss 1979;68:210.
[9] Hoffman JD. Polymer 1982;23:656.
[10] Dasari A, Rohrmann J, Misra RDK. Mater Sci Eng 2003;A360:237.
[11] Kristiansen M, Werner M, Tervoort T, Smith P, Blomenhofer M, Schmidt H-W. Macromolecules 2003;36:5150.
[12] Lustiger A, Marzinsky CH, Mueller RR. J Polym Sci Polym Phys 1998;36:2047.
[13] Bartczak Z. J Macromol Sci Phys 2002;B41(4–6):1205.

[14] Muratoğlu OK, Argon AS, Cohen RE, Weinberg M. Polymer 1995; 36:4787.
[15] Kim SH, Ahn SH, Hirai T. Polymer 2003;44:5625.
[16] Saujanya C, Radhakrishnan S. Polymer 2001;42:6723.
[17] Pozsgay A, Frater T, Papp L, Sajo I, Pukanszky B. J Macromol Sci Phys 2002;B41(4–6):1249.
[18] Gui Q, Xin Z, Zhu W, Dai G. J Appl Polym Sci 2003;88:297.
[19] He JD, Cheung MK, Yang MS, Qi Z. J Appl Polym Sci 2003;89:3404.
[20] Xu W, Ge M, He P. J Polym Sci Polym Phys 2002;40:408.
[21] Quian J, He P, Nie K. J Appl Polym Sci 2004;91:1013.
[22] Lin Z, Huang Z, Zhang Y, Mai K, Zeng H. J Appl Polym Sci 2004;91: 2443.
[23] Avrami M. J Chem Phys 1939;7:1103.
[24] Avrami M. J Chem Phys 1940;8:212.
[25] Jeziorny A. Polymer 1978;19:1142.
[26] Wunderlich B. Macromolecular physics. vol. 2. New York: Academic Press; 1976.
[27] Ozawa T. Polymer 1971;12:150.
[28] Liu T, Mo Z, Wang S, Zhang H. Polym Eng Sci 1997;37:568.
[29] García-Martínez JM, Laguna O, Areso S, Collar EP. Eur Polym J 2002;38:1583.
[30] Díez-Gutiérrez S, Rodrígues-Pérez MA, De Saja JA, Velasco JI. Polymer 1999;40:5345.
[31] Wunderlich B. Thermal analysis. New York: Academic Press; 1990. p. 418.
[32] Wunderlich B. J Therm Anal 1997;49:7.
[33] Arrighi V, McEwen IJ, Qian H, Prieto MBS. Polymer 2003;44:6259.
[34] Kissinger HE. J Res Natl Inst Stand 1956;57:217.
[35] Fillon B, Thierry A, Lotz B, Wittman JC. J Therm Anal 1994;42:721.
[36] Jain S, Goossens H, Picchioni F, Duin Mv. Accepted polymer 2005.
[37] Rotter G, Ishida H. Macromolecules 1992;25:2170.
[38] Gopakumar TG, Lee JA, Kontopoulou M, Parent S. Polymer 2002;43: 5483.
[39] Cebe P, Hond SD. Polymer 1986;27:183.
[40] Ziabicki A. Colloid Polym Sci 1974;252:433.
[41] Yu J, He J. Polymer 2004;41:891.
[42] Lee Y, Porter R. Macromolecules 1988;21:2770.
[43] Lorenzo ML, Silvestre C. Prog Polym Sci 1999;24:917.
[44] Lee SW, Cakmak M. J Macromol Phys 1998;B3:568.
[45] Cho K, Saheb DN, Choi J, Yang H. Polymer 2002;43:1407.
[46] It has to be noted that the X-ray wavelength used is 1.218 Å.